# CFD modelling and optimization of ammonia synthesis-absorption integrated reactor under mild conditions

Line Flansmose Olsen
Thermal Energy and Process Engineering, TEPE4-1009, 2025-10
Master Thesis





#### AALBORG UNIVERSITY

STUDENT REPORT

#### Title:

CFD modelling and Optimaization of ammonia synthesis-absorption integrated reactor under mild conditions

Theme:

**Master Thesis** 

**Project Period:** 

**Project Group:** TEPE4-1009

Participants:

Line Flansmose Olsen

Supervisors:

Vincenzo Liso Tianbao Gu

Number of Pages: 28

Date of Completion:

October 2th - 2025

#### Abstract:

In the Thesis, integrated absorption-enhanced ammonia synthesis is investigated using Computational Fluid Dynamics (CFD) integrated with two kinetic models that describe the synthesis and the absorption. The project is focused on modeling, validating, and optimizing a single-vessel reactor. The absorptionenhanced ammonia synthesis is proposed as a potential sustainable alternative to the conventional Haber Bosch process. The model is validated using experimental data found in the literature. And the accuracy of the CFD model is tested through a grid independence study. A parametric study showed that a configuration that incorporated multiple layers of catalyst and absorbent was capable of achieving hydrogen conversions comparable to those of a single pass in the Haber Bosch process, but at lower operating conditions. Multiple Object Optimization using the central composite design highlighted the critical role of gas hourly space velocity (GHSV) and reactor geometry in balancing conversion efficiency and absorption capacity. The findings confirm that CFD-based modeling is a viable tool for studying ammonia production under renewable energy-compatible conditions, while also emphasizing the need for further experimental validation and economic assessment.

AAU Energy Aalborg University http://www.aau.dk

# Summary

Ammonia plays a central role in both agriculture and industrial applications, and in recent years it has attracted renewed attention as a potential energy carrier for Hydrogen storage. The conventional Haber–Bosch process, which has been the industrial standard for over a century, is a highly energy-intensive method, that relies heavily on fossil fuels, and accounts for approximately 1–2% of the global annual CO<sub>2</sub> emissions. These limitations have created an urgent demand for more sustainable alternatives. One promising direction is sorption-enhanced ammonia synthesis, where in-situ absorption of ammonia can shift the chemical equilibrium toward higher conversion rates at milder operating conditions. This thesis investigates the performance and optimization of such a system through computational fluid dynamics (CFD) modeling.

This project works with a CFD framework that couples two detailed kinetic models: one describing ammonia synthesis over a catalyst bed and the other describing ammonia absorption by manganese chloride supported on silica (MnCl<sub>2</sub>/SiO<sub>2</sub>). This absorbent was selected due to its high thermal stability and resistance to acid formation. The reactor was modeled as a single-vessel, integrated system where the synthesis and absorption zones are combined. The CFD model was implemented in Ansys Fluent and validated against experimental data from the literature, while a grid independence study was carried out to ensure numerical reliability.

Parametric studies revealed that introducing layered catalyst–absorbent configurations significantly enhances the hydrogen conversion and ammonia yield under mild conditions. By adding additional catalyst and absorption layers, a H<sub>2</sub>-conversion of 15% was reached. The optimization component of the thesis focused on two critical design variables: the gas hourly space velocity (GHSV) and the reactor diameter. Using a central composite design (CCD) methodology, response surfaces were generated for both hydrogen conversion and ammonia absorption. The results demonstrated that GHSV is inversely proportional to both conversion efficiency and absorbed fraction, making it a decisive parameter in reactor operation. Reactor diameter also influenced performance by affecting saturation times and flow dynamics. A multi-objective genetic algorithm was employed to identify optimal operating points, yielding candidate solutions that balanced conversion efficiency with absorption capacity.

The findings demonstrate the viability of CFD modeling as a predictive and optimization tool for emerging ammonia synthesis technologies. Although the model was successfully validated with experimental data, uncertainties remain due to the lack of detailed reactor dimensions and operating parameters in the literature. These limitations emphasize the importance of continued experimental research to refine assumptions such as ideal gas behavior, neglect of intermediates, and thermal equilibrium conditions.

Overall, the thesis concludes that sorption-enhanced ammonia synthesis has the potential to become a sustainable and flexible alternative to the conventional Haber–Bosch process, especially when paired with renewable hydrogen sources. The integrated system offers advantages in scalability, lower operating conditions, and compatibility with decentralized production.

## **Preface**

#### **Reading Guide**

In this project the IEEE method was chosen used for citations. According to the IEEE method the citations used will be numbered according to appearance, and written as such [1]. The citations follow their references in the bibliography located at the end of the thesis. While when chapters, sections, figures, tables and equations are labeled these will also be references, to where they are mentioned in the text. The numbering of these labels follows in chronological order and chapters order. Throughout the report, some symbols and abbreviations may have different subscripts, however, these differences can be found in the Nomenclature.

The following software has been used in this project:

- Mathworks MATLAB
- Ansys Workbench
- Microsoft Excel
- Overleaf Latex
- Microsoft Power Point

Line Flansmose Olsen lfol20@student.aau.dk

Signature: Line Flansmose Obsen

The content of this report is freely available, but publication (with reference) may only be pursued due to agreement with the author.

By accepting the request from the fellow student who uploads the study group's project report in Digital Exam System, you confirm that all group members have participated in the project work, and thereby all members are collectively liable for the contents of the report. Furthermore, all group members confirm that the report does not include plagiarism.

# Nomenclature

#### Standard SI-Units will be used

Symbol	Explanation	Unit
A	Pre-exponential factor $\frac{\text{kmol}}{\text{m}^3.\text{h}}$	
$a_i$	Activity	[-]
$C_2$	Inertial loss coefficient	[-]
$c_p$	Specific heat capacity	$\left[\begin{array}{c} J \\ \overline{\text{kg.K}} \end{array}\right]$
D	Prescribed matrix	
d	Diameter	[m]
E	Total energy	$\left[ \frac{J}{kg} \right]$
$E_a$	Activation energy	
$e^{(a)}$	Approximated error	[%]
$e^{(ext)}$	Extrapolated error	[%]
f	Fugacity	[atm]
$H_{vap}$	Vaporization enthalpy	$\left[\begin{array}{c} J \\ \overline{kg} \end{array}\right]$
h	Cell size	[m]
$h_j$	Specific enthalpy	
J	Diffusive flux	$\frac{\text{mol}}{m^2 \cdot s}$
K	Equilibrium constant	[-]
k	Rate constant	$\frac{\text{kmol}}{\text{m}^3.\text{s}}$
$k_i$	Thermal conductivity	$\left[\frac{W}{m.K}\right]$
MW	Molecular weight	$\left[\frac{g}{mol}\right]$
N	Number of cells	[-]
p	Pressure	[Pa]
p <sub>GCI</sub>	Apparent order	[-]
Q	Energy	[W]
R	Universal gas constant	$\left[J.\text{mol}^{-1}.\text{K}^{-1}\right]$
r	Refinement factor	[-]
R <sub>abs</sub>	Sorption reaction rate	$\begin{bmatrix} \frac{\text{mol}}{g_{\text{MnCl}_2}.\text{min}} \end{bmatrix}$
$R_{ m NH_3}$	Synthesis reaction rate	kmol m <sup>3</sup> .h
S	Source term	[-]
$S_m$	Mass source term	$\left[\frac{kg}{m^3.s}\right]$
$S_h$	Energy source term	$\left[\frac{W}{m^3}\right]$
T	Temperature	[K]
t	Time	[s]
v	Velocity	
V	Volume	$\lceil m^3 \rceil$
$x_i$	Mole fraction	[-]
$X_a$	Sorption capacity index	[-]

#### **Greek Letters**

Symbol	Explanation	Unit
Y	Mass fraction	[-]
α	Correction factor	[-]
$\alpha_p$	Permeability	[m <sup>2</sup> ]
Γ	Diffusion coefficient	[-]
γ	Porosity	[-]
$\gamma_j$	Activity coefficient	[-]
$\epsilon$	Void fraction	[-]
θ	Angle	[°]
μ	Dynamic viscosity	$\left[\frac{kg}{m.s}\right]$
ρ	Density	$\left[\frac{kg}{m^3}\right]$
$\bar{ au}$	Viscous stress tensor	[-]
φ	Scalar	[-]

Symbol	Explanation
0	Standard condition
1, 2	Index
abs	Absorption
ст	Coarse mesh/medium mesh
domain	Domain
eff	Effective
eq	Equilibrium
ext	Extrapolated
f	Fluid
fine	Fine
h	Heat
i	Index direction
in	Inlet
j	Index species
т	Mass
max	Maximum
medium	Medium
mf	Medium mesh/fine mesh
min	Minimum
momentum	Momentum
out	Outlet
p	Particle
r	Reactor
rxn	Reaction
S	Solid
sorbent	Sorbent
total	Total
vap	Vaporization

#### Abbreviations

Abbreviation	Explanation
2D	Two Dimensional
3D	Three Dimensional
CCD	Central Composite Design
CFD	Computational Fluid Dynamics
DOE	Design Of Experiment
GCI	Grid Convergence Index
GHSV	Gas Hourly Space Velocity
MOGA	Multi-Objective Genetic Algorithm
UDE	User Defined Expression
UDS	User Defined Scalar

# **Contents**

1	ntroduction	1		
	1.1 Motivation	1		
	1.2 The conventional Haber-Bosch process	1		
	1.3 State of the art	2		
2	Project Objective			
3	Methodology	6		
	3.1 Kinetic model	6		
	3.1.1 Modeling of the Ammonia Synthesis	6		
	3.1.2 Absorption model	7		
	3.2 CFD model	9		
	3.2.1 Geometry	10		
	3.2.2 Meshing	10		
	3.2.3 Governing Equation	10		
	3.2.4 Integration of the kinetic models	11		
	3.2.5 Boundary Conditions and CFD Solution Methods	12		
4	Results and Discussion	14		
	4.1 Validation and verification	14		
	4.1.1 Grid independence study	14		
	4.1.2 Validation	15		
	1.2 Parametric study	15		
	4.3 Optimization	17		
5	Conclusion 2			
6	Future Work 22			
Bi	liography	22		
A	Geometry script	25		
В	User Defined Expressions 2			
	Ontimaztion Canidate Points	28		
•	JOHNSKION CANIDATE POINTS	_/X		

## Chapter 1

## Introduction

#### 1.1 Motivation

Ammonia is an important part of modern food production and industry processes, but it also has potential as a carrier of renewable hydrogen [1]. The production of ammonia is primarily done through the Haber-Bosch process [2]. However, the Haber Bosch process is an energy-intensive method that is reliant on fossil fuels, making it responsible for approximately 1-2% of global annual CO<sub>2</sub> emissions[3]. It is therefore essential to find alternative methods that can operate under milder conditions and are compatible with hydrogen produced from renewable energy sources.

One of the methods that has shown promising results is the use of absorption-enhanced processes [3]. By having absorption, it is possible to shift the reaction equilibrium, thereby improving the yield while operating at lower temperatures and pressures [3]. The conventional Haber-Bosch process requires a continuous and large-scale supply of hydrogen, which sustainable hydrogen sources cannot feasibly cover [3] [4]. The absorption-enhanced process is more suitable for integration with renewable hydrogen sources as its milder operating conditions offer greater scalability and flexibility.

Additionally, ammonia offers advantages as a hydrogen carrier, particularly in terms of transportation and storage. The transportation and storage of hydrogen is a challenge, this is due to its low boiling point (-252.8 °C), therefore requiring high-pressure tanks or cryogenic temperatures for storage [1]. Ammonia, which has a higher boiling point (-33.8 °C) can be stored and transported in the already established infrastructure [1]. Compared to other hydrogen carriers, ammonia has a high hydrogen weight fraction (17,65%) [5]. The possibility of using ammonia to store energy further supports the case for the development of a decentralized ammonia production method that is compatible with renewable energy sources.

#### 1.2 The conventional Haber-Bosch process

In the conventional Habor-Bosch process, hydrogen and nitrogen are converted into ammonia (NH<sub>3</sub>) using a Fe-based catalyst at operating conditions of 400 to 500 °C and pressures >100 bar, due to thermodynamic limitations, the conversion remains below 20% [6]. After the reaction, the ammonia is separated through condensation, while the unreacted gases are fed back into the reactor (see Figure 1.1a). For ammonia to condensate, the gas mixture must be cooled to  $\approx -20$ °C, adding to the overall energy demand of the Haber-Bosch process [7].

For ammonia synthesis operating under mild conditions (300°C and 40–50 bar), separation through condensation becomes inefficient due to its high pressure requirement [6]. New

developments in absorption technology have emerged as a potential alternative to condensation, as it enables the separation of ammonia at lower pressures while achieving higher purity levels [6].

In current systems, this absorption process is carried out in a separate column downstream of the catalyst bed (see Figure 1.1b). Here, the sorbent material used for the absorption is regenerated through heating and pressure reduction, which releases the captured ammonia [7]. To further improve efficiency, ongoing research is focused on integrating the catalyst and sorbent beds within a single reactor (see Figure 1.1c) [6]. This in-situ sorption approach aims to shift the chemical equilibrium by spatially layering the catalyst and sorbent materials, thereby enhancing ammonia conversion rates [6].

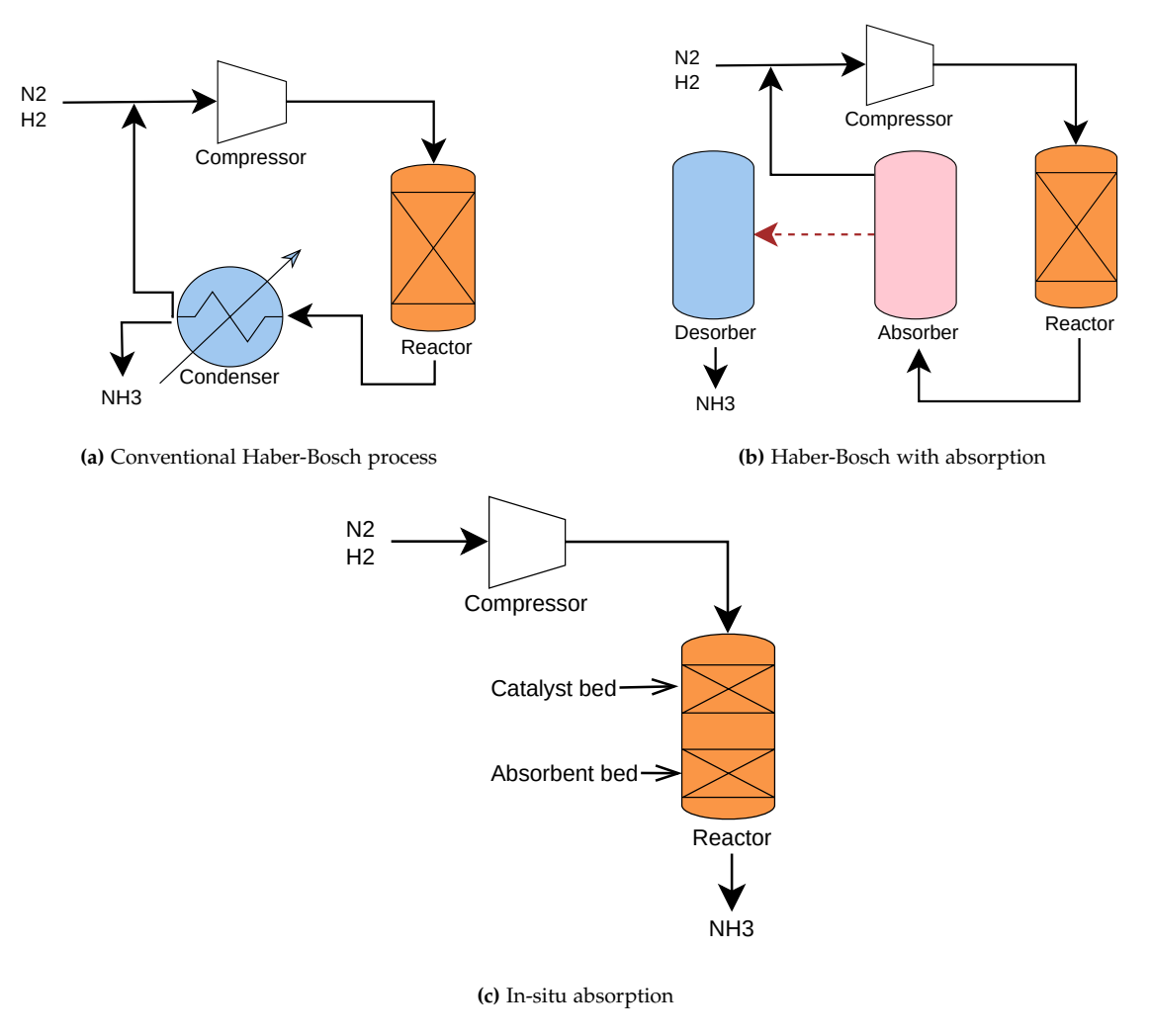


Figure 1.1: Ammonia synthesis methods [8]

#### 1.3 State of the art

The interest in the absorption enhanced Haber Bosch process operating under mild conditions has in recent years been intensified [9]. The research has led to the development of novel in-situ sorption reactor configurations [2]. Using sorption compared to condensation for the separation of ammonia allows a lower operational pressure while achieving a

cleaner separation of the ammonia [10].

Under the mild operating condition the selection of the catalyst plays a critical role for the efficiency of the reactor.

Researchers have during last decade been developing Ruthenium-based catalysts with activities that are superior under low temperatures and low pressures, compared to the Febased catalyst, that are commonly used in the conventional Haber Bosch process [11] [11]. However, the Ruthenium-based catalysts are more expensive, fragile, and less dense compared to the commercialized Fe-based catalysts [11]. Smith and Torrente-Murciano have therefore conducted a study comparing a Ruthenium-based catalyst (5%Ru/10%Cs/CeO<sub>2</sub>) to a commercialized cobalt-promoted catalyst Fe (KATALCO 74-1), which has been proven to perform well at lower temperatures and lower pressures (~ 80 bar) while maintaining good stability [11]. The study was conducted in a single-vessel with MnCl<sub>2</sub>/SiO<sub>2</sub> as the sorbent, with operating conditions down to 300°C and 20bar, showed that when looking at the total mass and volume of the reactor KATALCO 74-1 is competitive with the Ruthenium-based catalyst.[11] Further research is still needed, but the findings of the study by Smith and Torrente-Murciano shows an incentive to look further into commercialized catalysts rather than novel catalysts for absorption-enhanced ammonia production [11].

For the separation of ammonia, researchers have been looking into solid absorbents, as they are more selective and have a higher capacity at higher temperatures, compared to adsorbents [2]. One study that has been looking into the separation of ammonia using solid absorption was conducted by Malmali et al. [2]. The study was an experimental evaluation of different metal-halides (MgCl<sub>2</sub>, CaCl<sub>2</sub>, SrCl<sub>2</sub>, MgBr<sub>2</sub>, CaBr<sub>2</sub>, SrBr<sub>2</sub>) performance as ammonia absorbents [2]. The findings of the study showed that bromide-based salts had a higher capacity than the chloride-based salts [2]. However, it was concluded that chloridebased salts would probably be preferable in the real world, as they are cheaper and have the same ammonia capacity per mass [2]. Another finding from the study was that using porous material (silica, zeolite Y) to support the metal-halides had a positive effect on the capacity of the absorbent [2].  $MgCl_2$  and  $CaCl_2$  are among the conventionally used absorbents for ammonia separation due to their high capacity [6]. Studies have shown that the production rate of the conventional Haber Bosch process can be reached at lower pressures using CaCl<sub>2</sub> as an absorbent [12] [13]. For a single vessel reactor, combining catalyst and absorbent, CaCl<sub>2</sub> is unsuitable, due to unreasonable pressure requirements for the ammonia absorption, when the temperature is above 300 °C [6]. Even though MgCl<sub>2</sub> is able to absorb ammonia at temperatures up to  $\sim 400^{\circ}$ C, the absorbent starts to decompose at temperatures above 300°C in the presence of water. The decomposition causes acidic byproducts, which are harmful to both the catalyst and the absorbent [6] [10].

To prevent degradation in the integrated system, a more resilient absorbent cable that absorbs ammonia at relatively high temperatures is needed. An absorbent that meets these criteria is Manganese chloride supported by silica (MnCl<sub>2</sub>/SiO<sub>2</sub>) [6]. MnCl<sub>2</sub>/SiO<sub>2</sub> desorbs water at 200° C eliminating the risk of acid formation, at temperatures above [6]. In a study conducted by Smith and Torrente-Murciano an integrated single vessel reactor using a Ruthenium-based (5%Ru/10%Cs/CeO<sub>2</sub>) catalyst and MnCl<sub>2</sub>/SiO<sub>2</sub> as the absorbent, was successfully achieved with a conversion surpassing the equilibrium for a

single pass [6].

This study aims to utilize Computational Fluid Dynamics (CFD) as a tool for investigating and optimizing the geometry and the gas hourly space velocity (GHSV) in a single-vessel ammonia synthesis reactor with absorption. In the existing literature, CFD has primarily been employed to investigate catalysts in ammonia synthesis without absorption [14] [15] [16]. However, no CFD studies have reported on systems that combine both a catalyst and an absorbent within the same vessel. In a previous semester project, this configuration was explored, focusing on optimization of the operating pressure and the catalyst-to-absorbent bed length ratio [8]. It also explored the effect of adding a catalyst and absorbent layer in the vessel on H2 conversion and the amount of ammonia produced. The present work extends this line of research by examining geometric parameters and GHSV.

# Chapter 2

# **Project Objective**

The objectives of this project are:

- 1. Investigate NH<sub>3</sub> synthesis using a sorption-enhanced reactor.
- 2. Validate reactor design through modeling and data comparisons with existing data from the literature.
- 3. Assess the scalability of the synthesis-sorption unit.

## **Chapter 3**

# Methodology

This chapter presents the kinetic models used to describe the ammonia synthesis and ammonia absorption processes. Furthermore, the implementation in the CFD model is described.

#### 3.1 Kinetic model

Firstly, the global reaction for ammonia synthesis is presented:

$$N_2 + 3H_2 \rightleftharpoons 2NH_3$$
  $\Delta H_{rxn}^{\circ} = -46.22 \left[ \frac{kJ}{mol} \right]$ 

#### 3.1.1 Modeling of the Ammonia Synthesis

To model the ammonia synthesis, the Temkin's kinetic model is used [17]. This model assumes that the rate-determining step is the chemisorption of nitrogen. The reaction rate expression for the iron-based catalyst is described in equation 3.1 [18].

$$R_{\text{NH}_3} = 2 \cdot k \cdot \left( K_a \cdot a_{\text{N}_2} \cdot \left( \frac{a_{\text{H}_2}^3}{a_{\text{NH}_3}^2} \right)^{\alpha} - \left( \frac{a_{\text{NH}_3}^2}{a_{\text{H}_2}^3} \right)^{1-\alpha} \right) \left[ \frac{\text{kmol}}{\text{m}^3 \cdot \text{h}} \right]$$
(3.1)

Here  $\alpha$  is the correction factor, for ammonia synthesis, this is assumed to be 0.5 [19]. k is the reaction rate constant.  $K_a$  is the equilibrium constant, while  $a_i$  is the activity of each component.

The reaction rates of the individual components, shown in Equation 3.2, can be written according to their stoichiometric coefficient of the global reaction.

$$-R_{N_2} = -\frac{1}{3}R_{H_2} = \frac{1}{2}R_{NH_3} \left[ \frac{\text{kmol}}{\text{m}^3 \cdot \text{h}} \right]$$
 (3.2)

The equilibrium constant,  $K_A$ , for ammonia synthesis is expressed as equation 3.3 [20].

$$\log_{10} K_A = -2.691122 \cdot \log_{10} T - 5.519265 \cdot 10^{-5} T + 1.848863 \cdot 10^{-7} T^2 + 2001.6 T^{-1} + 2.6899$$
(3.3)

The rate constant, *k*, is found using the Arrhenius equation 3.4 [19].

$$k = A \cdot exp\left(-\frac{E_a}{RT}\right) \tag{3.4}$$

Where A is the pre-exponential factor with a value of  $8.849 \cdot 10^{14} [kmol/(m^3h)]$ ,  $E_A$  is the Activation energy = 170560 [kJ/kmol], and R is the universal gas constant  $[J/(mol \cdot K)]$ 

How the activity,  $a_j$ , which describes the effective concentrations and partial pressures of the individual components, is calculated is shown in equation 3.5

$$a_j = \frac{f_j}{f_i^0} \tag{3.5}$$

 $f_j$  is the fugacity component j. The fugacity is the effective pressure as it considers the behavior of non-ideal gases.  $f_j^0$  is the standard state fugacity. This is often the fugacity when the pressure is 1 bar.

Equation 3.6 shows how the fugacity is calculated.

$$f_j = x_j \cdot \gamma_j \cdot P \tag{3.6}$$

Here,  $x_j$  is the molar fraction of component j,  $\gamma_j$  is the activity coefficient of component j, and P is the total pressure.

The activity coefficient of Hydrogen is calculated using Equation 3.7. The units of the temperature *T* are here in Kelvin, while the pressure *P* is in atm. [19] [21]

$$\gamma_{\rm H_2} = exp \left( e^{(-3.4803 \cdot T^{0.125} + 0.541)} P - e^{(0.1263 \cdot T^{0.5} - 15.980)} P^2 + 300 \cdot e^{(0.0119 \cdot T - 5.941)} \cdot e^{(-P/300)} \right)$$
(3.7)

The activity coefficient of Nitrogen is shown in Equation 3.8.

$$\gamma_{N_2} = 0.93431737 + 0.3101804 \cdot 10^{-3} \cdot T + 0.2958961 \cdot 10^{-3} \cdot P - 0.2707279 \cdot 10^{-6} \cdot T^2 + 0.4775207 \cdot 10^{-6} \cdot P^2$$
(3.8)

And the activity coefficient of ammonia is found using equation 3.9.

$$\gamma_{\text{NH}_3} = 0.1438996 + 0.2028538 \cdot 10^{-2} \cdot T - 0.4487672 \cdot 10^{-3} \cdot P - 0.1142945 \cdot 10^{-5} \cdot T^2 + 0.2761216 \cdot 10^{-6} \cdot P^2$$
(3.9)

#### 3.1.2 Absorption model

After ammonia is synthesized in the catalyst bed, the gas flows into the absorption bed, where it encounters a sorbent composed of 50 wt% manganese(II)chloride supported on silica gel (MnCl<sub>2</sub>/SiO<sub>2</sub>). This material was selected for its suitability to the operating conditions of the project, with its high thermal stability at elevated temperatures. Unlike traditionally used sorbents such as MgCl<sub>2</sub> and CaCl<sub>2</sub>, MnCl<sub>2</sub> does not experience acid formation above 200 °C [6]. Other chlorides can generate acidic species in the presence of water, which can harm the catalyst and cause it to degrade. However, MnCl<sub>2</sub> desorbs water at around 190 °C, thus minimizing the risk of acid formation [6]. The combination of thermal stability, effective ammonia absorption capabilities, and no acid formation at temperatures above 200 degrees makes MnCl<sub>2</sub> especially suitable for an in-situ absorption ammonia synthesis reactor.

The sorption is modeled according to Smith and Torrente-Murciano [6]. The sorption in the modeling is divided into 3 steps. Figure 3.1 shows a visual representation of the 3 steps is shown in figure 3.1. The first step is the adsorption, where the ammonia binds

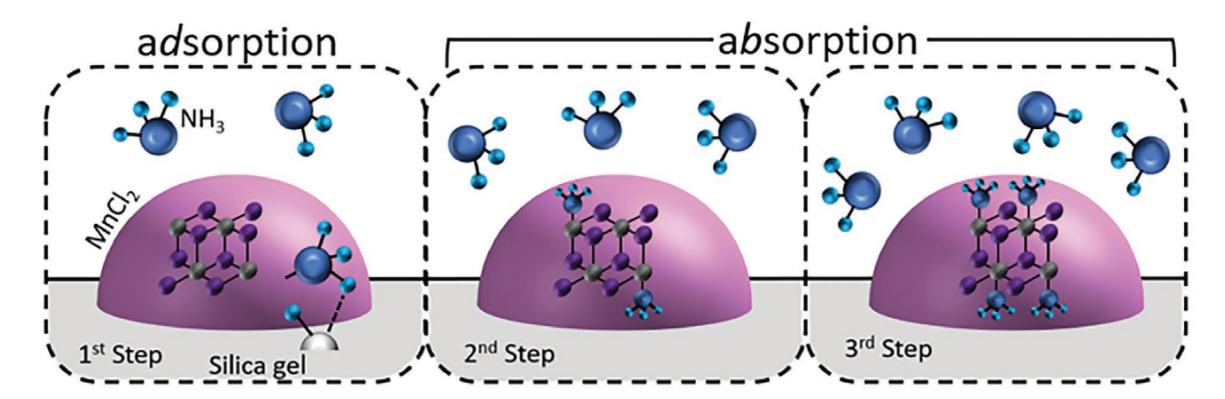


**Figure 3.1:** Illustration of the 3 steps of sorption that Smith and Torrente-Murciano divides the absorption of NH<sub>3</sub> into, in their absorption model for MnCl<sub>2</sub> [6].

itself to the surface of MnCl<sub>2</sub>.

The absorption reaction happening in the second step of the sorption model is described in Equation 3.10. While equation 3.11 shows the reaction in the 3rd step.

$$MnCl_2 + 0.5NH_3 \rightleftharpoons MnCl_2 \cdot 0.5NH_3 \tag{3.10}$$

$$MnCl_2 \cdot 0.5NH_3 + 0.5NH_3 \rightleftharpoons MnCl_2 \cdot NH_3$$
(3.11)

Equations 3.12 and 3.13 present the equilibrium constants,  $K_1$  and  $K_2$ , in terms of partial pressures for the absorption steps.

$$K_1 = \frac{1}{P_{eq1}^{0.5}} \tag{3.12}$$

$$K_2 = \frac{1}{P_{eq2}^{0.5}} \tag{3.13}$$

Van Hoff's equation is used to describe the equilibrium constants of the absorption steps, see equations 3.14 and 3.15.

$$\ln(K_1) = \frac{42100}{R} \left( \frac{1}{T} - \frac{1}{650} \right) \tag{3.14}$$

$$\ln(K_2) = \frac{42100}{R} \left( \frac{1}{T} - \frac{1}{610} \right) \tag{3.15}$$

The overall reaction rate of the absorption can be written as a summation of the reaction rates for three individual step.

$$R_{abs} = R_{abs}^{I} + R_{abs}^{II} + R_{abs}^{III} \left[ \frac{mol}{g_{\text{MnCl}_2} min} \right]$$
 (3.16)

The adsorption rate of the first step.

$$R_{abs}^{I} = 3 \cdot 10^{-4} (P_{\text{NH}_3} - 0.05) (1 - X_{A1}) \left[ \frac{mol}{g_{\text{MnCl}_2} min} \right]$$
 (3.17)

The rate of absorption in the second step.

$$R_{abs}^{II} = 2 \cdot 10^{-2} (P_{\text{NH}_3} - P_{eq1})^4 (1 - X_{A2})^4 \left[ \frac{mol}{g_{\text{MnCl}_2} min} \right]$$
(3.18)

The rate of absorption in the third step.

$$R_{abs}^{III} = 2.5 \cdot 10^{-2} (P_{\text{NH}_3} - P_{\text{eq}_2})^4 (1 - X_{A3})^6 \left[ \frac{mol}{g_{\text{MnCl}_2} min} \right]$$
(3.19)

#### 3.2 CFD model

For modeling, a CFD approach was chosen. Both a 2D and 3D model of an ammonia synthesis reactor with in-situ absorption were conducted.

The construction of the CFD model consists of the following parts:

- 1. Geometry: In the model the reactor is divided into 4 zones:
  - Inlet, here no reactions occur;
  - Catalyst bed, this is the part where the Ammonia synthesis reaction occurs;
  - Absorption bed, here the absorption of the ammonia is happening;
  - Outlet, no reactions occurring;
- 2. Mesh: Generating a high-quality mesh is important for accurate results.
- 3. Setup: Here boundary conditions, material properties, the gas composition, the kinetic model of the ammonia synthesis, and the absorption are defined.

Assumptions were made during the modeling, which are listed below.

- Intermediate species are neglected i.e. the mixture is considered only to consist of the three species:  $N_2$ ,  $H_2$ , and  $NH_3$ .
- The species are all assumed to behave as ideal gases and the properties of the mixture are defined by the ideal gas law.
- It is only the global reaction is accounted for in the catalyst bed.
- The thermal equilibrium is assumed to be between the solid and the gas phases.
- · Gravitational forces are not taken into account
- The cross-sectional area of the reactor is assumed to be uniform

#### 3.2.1 Geometry

The reactor is modeled as a cylinder with a diameter of 30 mm and a total length of 150 mm. The cylinder is divided into four sections: inlet, catalyst bed, Absorption bed and outlet. In Figure 3.2 a sketch with the measurements of the geometry is shown.

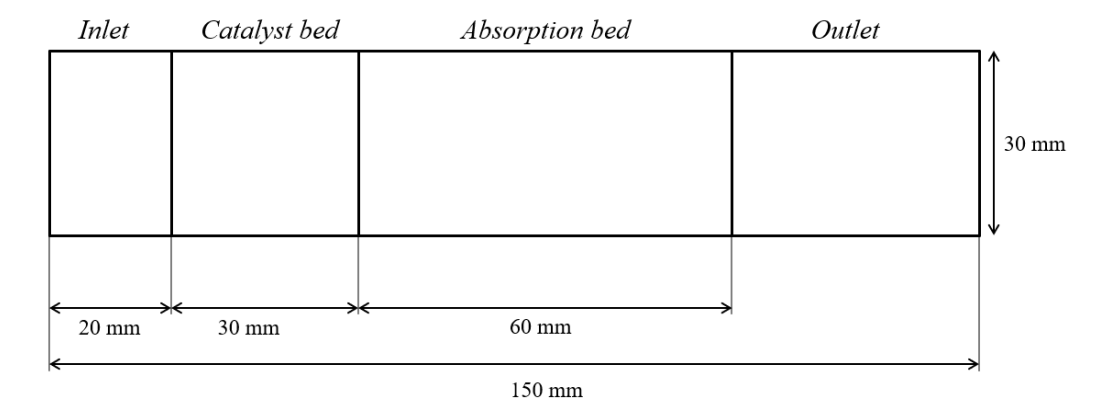


Figure 3.2: A sketch of the modeled geometry of the 1-layer model with the measurements

#### 3.2.2 Meshing

Having a high quality mesh is important for the accuracy of the results, since a poorly constructed mesh can lead to inaccuracies such as false diffussion [22]. To verify the quality of the meshes a grid independence study was conducted.

#### 3.2.3 Governing Equation

Both the catalyst bed and the absorption bed are packed beds, so to account for the influence that this has on the heat transfer and flow resistance, the beds are modeled as porous zones. In the model, its assumed that the porous zones are uniform and isotropic, so the porosity and the flow resistance are the same in all directions [23]. The CFD solver solves at set of governing equations describing the flow, by accounting for mass, momentum and energy conservation. By solving the governing equations the CFD solver can give a thorough description of the flow field inside the reactor.

Equation 3.20 is the general transport equation through a porous medium, as it is solved in Ansys Fluent, written using transient, convection, diffusion and source terms, in terms of scalar  $\phi$  [23].

$$\frac{\delta(\rho_f \phi \gamma)}{\delta t} + \nabla \cdot (\rho_f \vec{v} \phi) = \nabla \cdot (\gamma \Gamma_\phi \nabla \phi) + \gamma S_\phi$$
 (3.20)

 $\rho_f$  describes the fluid density,  $\gamma$  is the porosity of the medium, t is the time, while  $\vec{v}$  is velocity vector,  $\Gamma_{\phi}$  represents the diffusion coefficient and  $S_{\phi}$  is the source term [23]. In porous zones, the momentum equation uses additional source terms to describe inertial and viscous resistance, which can be expressed as 3.21.

$$S_{momentum,i} = -\left(\sum_{j=1}^{3} D_{ij} \cdot \mu_{f} \cdot v_{j} + \sum_{j=1}^{3} C_{ij} \cdot \frac{1}{2} \cdot \rho_{f} \cdot |v| \cdot v_{j}\right)$$
(3.21)

Here  $S_{momentum,i}$  is the momentum source term in the ith direction (i.e. x, y or z),  $\mu_f$  is the fluids dynamic viscosity and |v| is the magnitude of the velocity. Parameters C and D are prescribed matrices [23].

The momentum source terms, Equation 3.21, can be simplified for homogeneous porous zones, Equation 3.22, as the resistance becomes uniformly distributed [23].

$$S_{momentum,i} = -\left(\frac{\mu_f}{\alpha_p}v_i + C_2 \cdot \frac{1}{2} \cdot \rho_f \cdot |v| \cdot v_j\right)$$
(3.22)

 $\alpha_p$  is the permeability in the porous zone and is calculated using Equation 3.23 [23].

$$\alpha_p = \frac{d_p^2}{150} \frac{\epsilon^3}{(1 - \epsilon)^2} \tag{3.23}$$

The parameter  $C_2$ , from Equation 3.22, is inertial loss coefficient and is defined as Equation 3.24

$$C_2 = \frac{3.5}{d_p^2} \frac{1 - \epsilon}{\epsilon^3} \tag{3.24}$$

Here  $\epsilon$  is the void fraction of the bed and  $d_p$  is the particle diameter of either the catalyst or sorbent [23].

The Energy transport equation, Equation 3.25, is used to predict the temperature distribution and thermal behavior of the flow inside the reactor. In this model, the energy transport equation predicts this behavior by incorporating the convective and conductive heat transfer of the flow. It is here assumed that the solid and the fluid in porous zones are at thermal equilibrium [23].

$$\frac{\delta}{\delta t}(\gamma \rho_f E_f + (1 - \gamma)\rho_s E_s) + \nabla \cdot (\vec{v}(\rho_f E_f + p)) = \nabla \cdot (k_{eff} \nabla T - \sum_j h_j J_j + \bar{\tau}\vec{v}) + S_f^h \quad (3.25)$$

 $E_f$  is the total energy of the fluid,  $E_s$  is total energy of the solid,  $S_f^h$  is the fluid enthalpy source term, T is the temperature, while  $h_j$  and  $J_j$  is the specific enthalpy and diffusive flux, respectively, of species j and  $\bar{\tau}_{eff}$  is the effective viscous stress tensor [23].  $k_{eff}$  effective thermal conductivity, and is defined as Equation 3.26.

$$k_{eff} = \gamma k_f + (1 - \gamma)k_s \tag{3.26}$$

Where  $k_f$  is the thermal conductivity of the fluid and  $k_s$  is the thermal conductivity of the solid.[23]

#### 3.2.4 Integration of the kinetic models

In Ansys Fluent the kinetic model of the catalyst bed, described in Section 3.1.1, is incorporated using User Defined Expresses (UDE's). By using UDE's it is possible to specify

the mass source terms for the individual species, together with an energy source term that accounts for heat generated from the reaction. The UDE's implemented in the Ansys model stem from the HYSTRAM research project [24]. The specific UDE's implemented in the model can be found in Appendix B.

The mass source term in the general transport equation 3.20, for the individual species  $NH_3$  and  $H_2$  are diffined in Equations 3.27 and 3.28, respectively.

$$S_{\text{NH}_3} = R_{\text{NH}_3} \cdot MW_{\text{NH}_3} \tag{3.27}$$

$$S_{\rm H_2} = R_{\rm H_2} \cdot MW_{\rm H_2}$$
 (3.28)

Here  $MW_i$  is the molecular weight and  $R_i$  is the reaction rate of species i. The total mass source term is set to  $S_{tot} = 0$  as its assumed that there is no accumulations happening in the catalyst bed.

Equation 3.29 describes energy source term, accounts for the heat generated by the exothermic reaction.

$$S_{h,rxn} = -R_{\text{NH}_3} \cdot \Delta H_{rxn}^{\circ} \tag{3.29}$$

Incorporating the kinetic model for the absorption, described in section 3.1.2, in Ansys Fluent, is done by the use of UDE's to describe the mass and energy source terms. To implement the reaction rates of the absorption User Defined Scalars (UDS's) are used. The UDS's are additional transport equations, that describes the sorption capacity in each of the sorption steps. The transport equation for the scalars neglects the diffusion and convection terms, the transport equation for the UDS can therefor be described as Equation 3.30.

$$\frac{\delta(\rho_f \phi)}{\delta t} = S_{\phi} \tag{3.30}$$

As the absorbent only absorbs ammonia, is the total mass source term for the absorbent equal to NH<sub>3</sub> mass source term, described in equation 3.31.

$$S_m^{abs} = -R_{abs} \cdot MW_{\text{NH}_3} \cdot \rho_{sorbent} \tag{3.31}$$

Where  $\rho_{sorbent}$  is the bulk density of the sorbent. While the source terms for  $H_2$  and  $N_2$  are  $S_{H_2}^{abs}=0$  and  $S_{N_2}^{abs}=0$ 

The energy source term for the absorption, is shown in equation 3.32

$$S_{h,rxn} = -R_{abs} \cdot \Delta H_{abs}^{\circ} \tag{3.32}$$

Here  $R_{abs}$  the absorption reaction rate and  $\Delta H_{abs}^{\circ}$  is the absorption reaction enthalpy.

#### 3.2.5 Boundary Conditions and CFD Solution Methods

Figure 3.3 shows the boundary conditions used for the setup in ansys of the base case scenario. It is important for the accuracy of the CFD model to choose appropriate boundary conditions. At the inlet the temperature, molar fractions of the three species and the velocity are defined. At the outlet outflow has been chosen as boundary condition as it

Operating pressure: 40 bar

allows for the internal flow dynamics to determine pressure at the outlet. The boundary condition at walls are assumed to be isothermal. This assumption was made to ensure that internal temperature of the reactor would not increase above  $400^{\circ}$ C, due to the absorption model only being valid below  $400^{\circ}$ C [6].

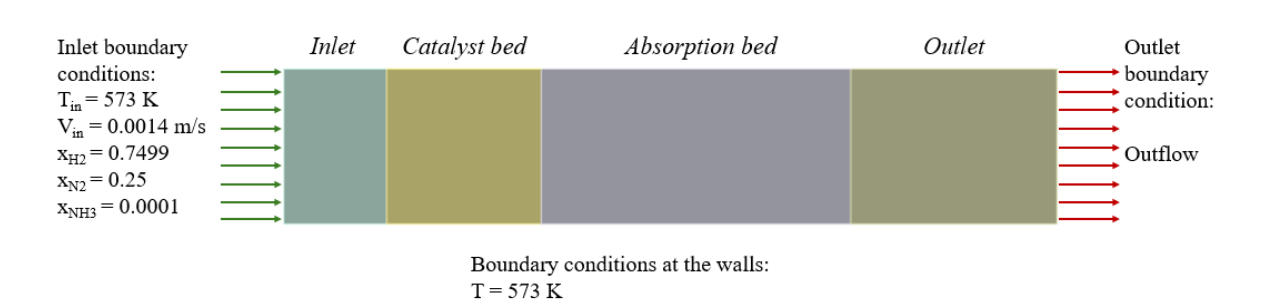


Figure 3.3: Illustration of the reactor with the boundary conditions for the base case

Table 3.1 list the CFD methods chosen in the developed model.

Table 3.1: CFD Methods

Settings	Description
Included models	2D planar transient laminar model with species transport and porous zones
Solving Algorithm	Coupled Algorithm
Discretization Schemes	2nd order Upwind; 2nd order Implicit
Solver	Ansys Fluent 2025 R1

The couple algorithm was chosen for handeling the presure-velocity coupling, as its simultaneous solving of the pressure and the velocity across the flow domain allows for better convergence and stability compared to other schemes [25]. For the spatial discretization, the 2nd-order upwind scheme was chosen, as it provides a more accurate solution compared to the 1st-order upwind scheme [25]. Lastly was the 2nd order Implicit scheme chosen for the temporal scheme, because of its stability and accuracy [25].

## **Chapter 4**

## **Results and Discussion**

#### 4.1 Validation and verification

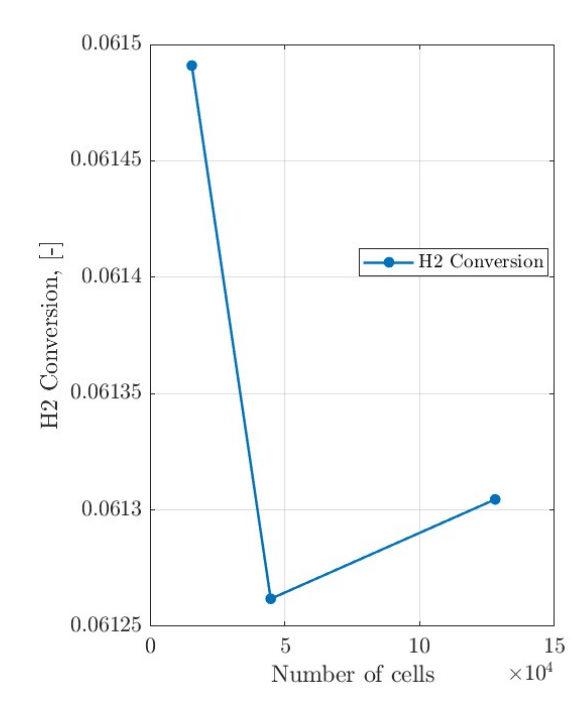
#### 4.1.1 Grid independence study

A way of verifying the results of a CFD model is to do a grid independence study. The grid independence study evaluates the quality of the mesh, so that inaccuracies in the results due to, for example, false diffusion are avoided [22]. For this study, the Grid convergence index (GCI) method was utilized for the verification of the CFD model. The GCI compares 3 meshes at different levels of refinement, i.e. a coarse, a medium and a fine mesh. For each of the meshes a key variable, of the solution, is chosen for the comparison. The calculation done through multiple, which are described by Celik et al. in [26], resulting in Equation 4.1.

$$GCI_{fine} = \frac{1.25 \cdot e_{mf}^{(a)}}{r_{mf}^{p_{GCI}} - 1} \tag{4.1}$$

Here  $e_{mf}^{(a)}$  is the approximated relative error between the medium and fine mesh,  $r_{mf}$  is the refinement factor between the medium and fine mesh, and  $p_{GCI}$  is the apparent order.

In this case the  $H_2$  conversion was chosen as the key variable, for the GCI study. The results of the study are presented in Table 4.1.



Parameters	Values	
$N_f, N_m, N_c$	128000, 44745, 15512	
$\mathbf{r}_{mf}$	1.698 [-]	
$\mathbf{r}_{cm}$	1.691 [-]	
$\phi_{fine}$	$6.130 \cdot 10^{-2}$ [-]	
$\phi_{medium}$	$6.126 \cdot 10^{-2}$ [-]	
$\phi_{coarse}$	$6.149 \cdot 10^{-2}$ [-]	
$p_{GCI}$	3.16 [-]	
$\phi_{mf}^{(ext)}$	$6.131 \cdot 10^{-2} [-]$	
$\phi_{cm}^{(a)}$	$6.121 \cdot 10^{-2} [-]$	
$e_{mf}^{(a)}$	0.0697 %	
$e_{mf}^{(ext)}$	0.0163 %	
$e_{cm}^{(a)}$	0.0861%	
$e_{cm}^{(ext)}$	0.374 %	
$GCI_{fine}$	0.0204 %	
$GCI_{medium}$	0.108 %	

**Figure 4.1:** Plot showing the NH<sub>3</sub> production as a function of number of cells

**Table 4.1:** The results of the GCI study on the H<sub>2</sub> Conversion of the 2D model

The GCI value for the fine and the medium mesh are both well below the 1% that indicates grid independence. It is also shown that the relative error, both the extrapolated and the approximated, between the medium and coarse and medium is below 0,5%, the coarse mesh therefore also assessed to be in the grid independent range. Based on the results of the GCI study, the coarse mesh is selected for the simulations, as it to provided accurate results at significantly lower computational costs compared to the medium and fine mesh.

#### 4.1.2 Validation

For the validation of the models capabilities to predict the conversion of ammonia, the experimental data reported by Smith and Torrent-Murciano [6] are used. In their experimental study of an absorption integrated ammonia synthesis reactor, the authors investigated the single-pass low-temperature activity of the commercialized Fe-based catalyst KATALCO 35-8A, with a  $3:1~H_2/N_2$  feed. From this experiment the conversion of ammonia was calculated from the outflow measurements, taken with a mass flow, and the NH3 mole fraction at the outlet, which was obtained by gas chromatography. Running the CFD model at the experimental pressure (20 bar), yielded a H2 conversion of 3.67% at  $300^{\circ}$ C, which is consistent with is consistent with experimental result. However, the article does not disclose the GHSV or the dimensions of the vessels. These unknowns does put an uncertainty on the validation as these values influences the conversion.

### 4.2 Parametric study

In the previous semester project, it was discovered that adding one layer of catalyst and one of absorbent had a significant effect on H<sub>2</sub> conversion and production of NH<sub>3</sub> [8].

An assessment on the amount of layers, it is possible to add before this effect becomes insignificant. The result of this study, is shown in figure 4.2.

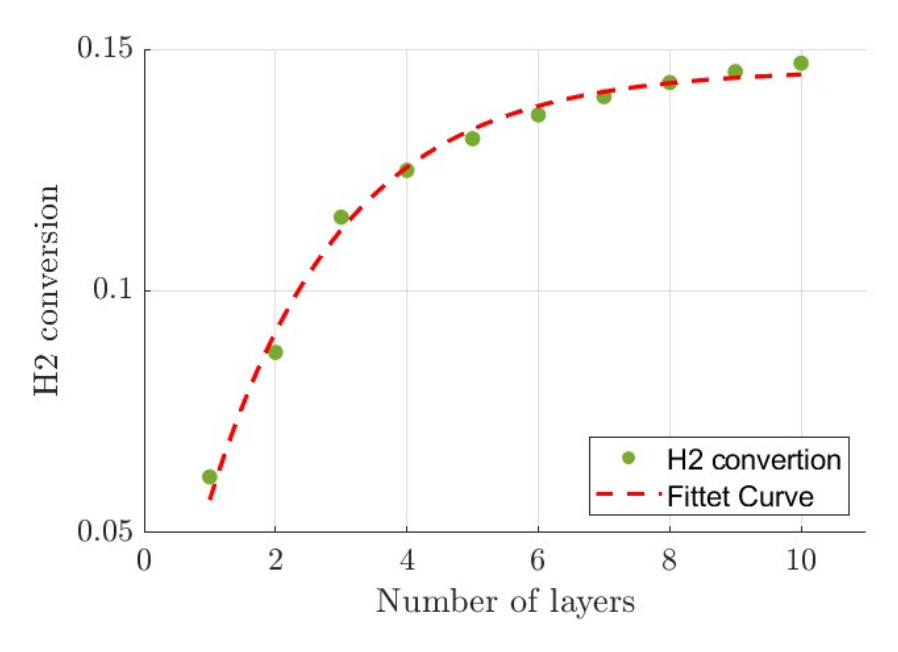


Figure 4.2: The H<sub>2</sub> conversion, after 6 minutes, as a function of catalyst and absorbent layers

After 4 layers the  $H_2$  conversion 13%, after which the effect of adding layers begins to stagnate. In comparison, the conversion of  $H_2$  in a single pass, in conventional Haber Bosch process, in the range of 15-20%, with 20 being the thermodynamic limit [27] [6]. Figure 4.3 shows the NH<sub>3</sub> production rate as a function of the catalyst-absorption layers.

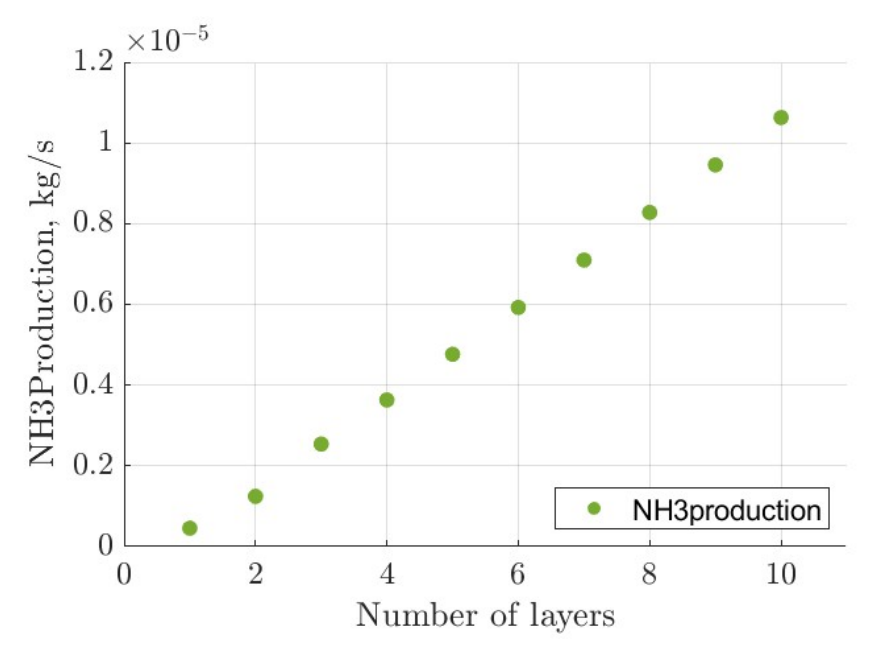
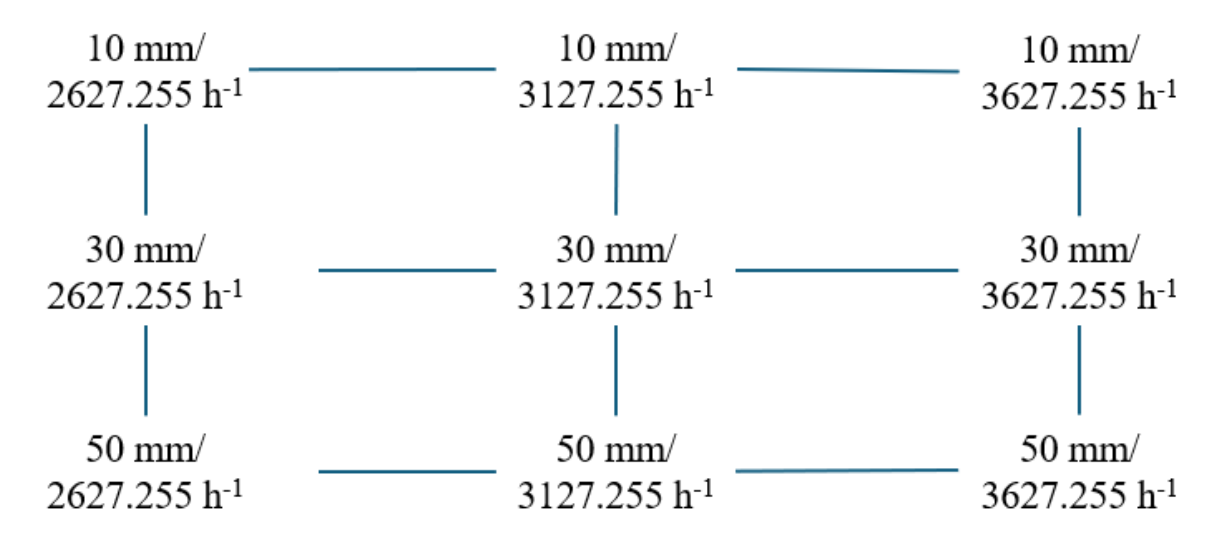


Figure 4.3: The ammonia production after 6 minute, as s function Catalyst and absorbent layers

Figure 4.3



**Figure 4.4:** Illustration of the Central Composite Design (CCD) with the 9 design points chosen for the optimization of the reactor diameter and the GHSV

#### 4.3 Optimization

When designing the in-situ absorption enhanced ammonia synthesis reactor the Gas Hourly Space Velocity (GHSV) and the diameter of the reactor, are two of the variables that influences both the cost and the efficiency of the reactor. In this study the effect of two variables on the H<sub>2</sub> conversion and the Absorption fraction is evaluated, making it a multiple object optimization problem. Using the centralized composite design (CCD) 9 design points were generated in Ansys workbench. Figure 4.4 shows the design points chosen for this optimization. All the design point was set to 10 minutes.

With the design points, response surfaces for  $H_2$  conversion and the  $NH_3$  absorbed fractions have been generated (See figures 4.6 and 4.5).

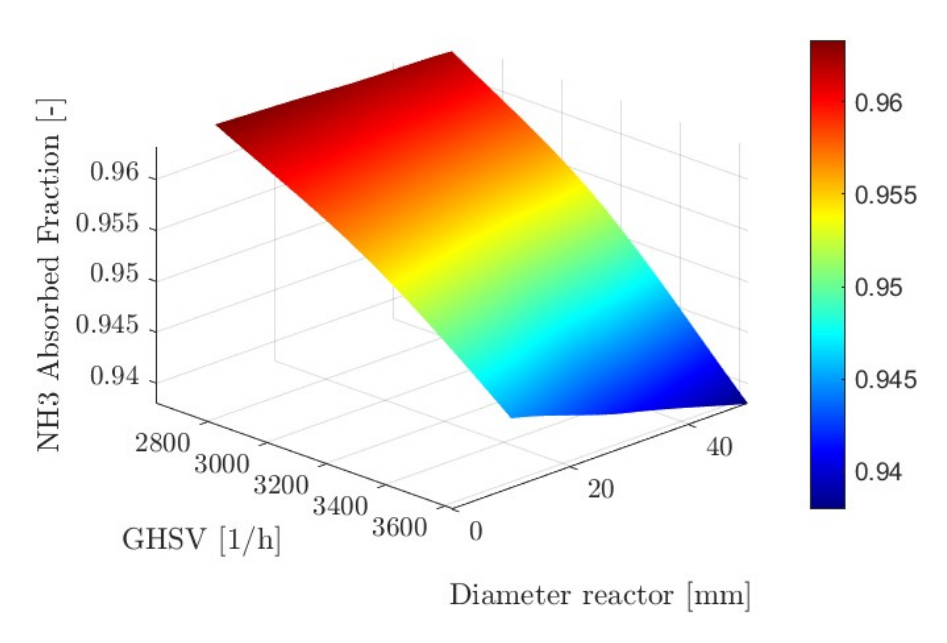


Figure 4.5: Response surface of the NH<sub>3</sub> absorbed fraction as a function of GHSV and reactor diameter

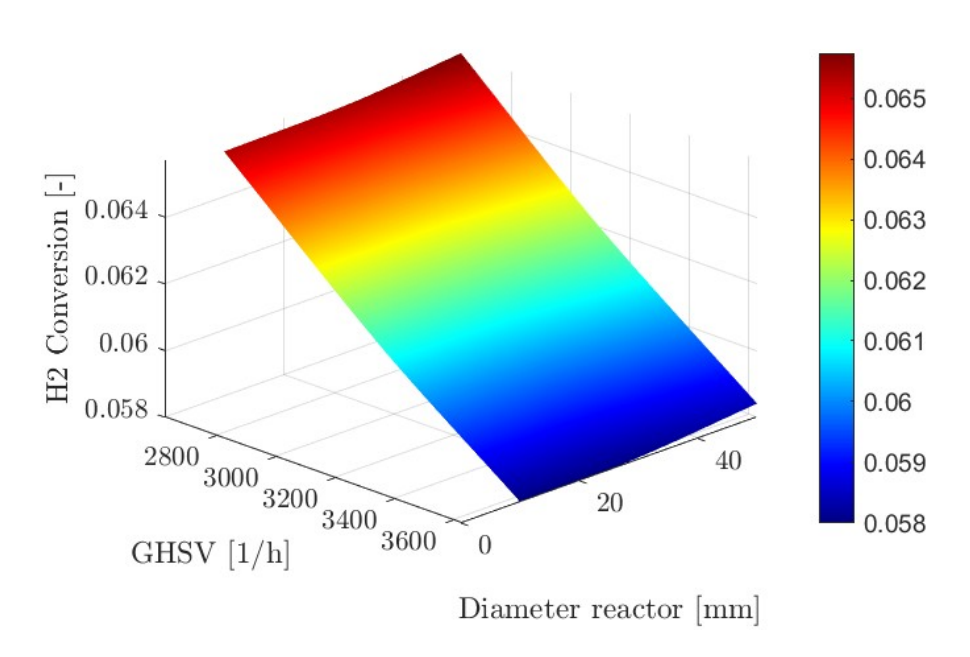


Figure 4.6: Response surface of the H2 conversion as a function of GHSV and reactor diameter

From the response surfaces it is shown that both the H<sub>2</sub>- conversion and the NH<sub>3</sub> Absorbed fractions are inversely proportional with the GHSV. In figure 4.5 the increase of diameter shortens the saturation time.

To find the optimal points of the response surfaces, mathematically. The design points are fitted by a quadratic regression model, which can accurately predict points on the response surface. The regression moddel for the NH<sub>3</sub> absorbed fraction is defined as  $f_1$ , while  $f_2$ 

represents the H<sub>2</sub>- conversion.

$$f_1(GHSV, d_r) = 0.931388 + (3.351848 \cdot 10^{-5}) \cdot GHSV + (3.413811 \cdot 10^{-4}) \cdot d_r - (1.444073 \cdot 10^{-7}) \cdot GHSV \cdot d_r - (8.096000 \cdot 10^{-9}) \cdot GHSV^2 + 3.019875 \cdot 10^{-7} \cdot d_r^2$$

$$(4.2)$$

$$f_2(GHSV, d_r) = 0.095617 - 1.451109 \cdot 10^{-5} \cdot GHSV - 9.897322 \cdot 10^{-6} \cdot d_r + 1.025250 \cdot 10^{-10} \cdot GHSV \cdot d_r + (1.145729 \cdot 10^{-9}) \cdot GHSV^2 + 3.310171 \cdot 10^{-7} \cdot d_r^2$$

$$(4.3)$$

By solving for the maxima of  $f_1$  and  $f_2$ , using the multi-objective generic algorithm, 35 candidate points for the optimal solution were obtained. The candidate points for GHSV vary from 2673  $[h^{-1}]$  to 2676  $[h^{-1}]$ . The diameter of the reactor varies from 19.1 mm to 44.1 mm. All the generated design points can be found in Appendix C, and 4 randomly selected is presented in 4.2.

GHSV	<b>Diameter</b> <sub>reactor</sub>	<b>Absorbed Fraction</b>	H <sub>2</sub> conversion
2627.3	31.177	0.9627	0.06542
2627.3	40.551	0.9625	0.06555
2627.5	42.880	0.9625	0.06559
2627.3	19.104	0.9630	0.06534

Table 4.2: Candidate points

The design points are quite close together, except for the diameter. This both due to both the range of the scope and the choice of optimizing for the Absorption fraction and H<sub>2</sub>conversion together, when they both increase when there is more time for the reaction. With the GHSV as one of the design points the NH<sub>3</sub> production rate and the H<sub>2</sub> conversion would probably have resulted in more variance in the candidate points.

## Chapter 5

# Conclusion

In this thesis, a computational fluid dynamics (CFD) framework was developed and coupled with two kinetic models, one describing ammonia synthesis and the other describing the absorption, with the purpose of investigate, validate, and optimize a single-vessel, integrated synthesis–absorption reactor.

The model was validated against the available experimental data, showing agreement with reported hydrogen conversion values. A Grid independence study was performed to prevent inaccuracies due to a poorly meshed grid. The result of the study indicated a three highly independent meshes, with the coarse mesh being chosen for subsequent calculations.

The parametric study, studying the influence of adding multiple catalyst- and absorption layers to the reactor proved that even under mild condition, it is possible to reach a conversion that can compete with the conventional Haber Bosch process. The results indicate that while the introduction of multiple catalyst-absorbent layers enhances conversion efficiency, the incremental gains decrease with each added layer.

The optimization study, which was conducted using a central composite design, high-lighted how influential the Gas Hourly Space Velocity (GHSV), is for the efficiency of the reactor. the study also showed how useful multi-objective optimization can be in integrated systems.

Even though the model was validated to experimental data, there were some limiting factors regarding the lack of knowledge about reactor geometry and operating conditions. These factors introduce uncertainty into the quantitative predictions. However, the methodology and findings presented form a solid foundation for continued refinement and experimental validation.

In conclusion, CFD modeling with sorption-enhanced kinetics demonstrates the potential for ammonia production under mild conditions. The results showed that there is still potential for further optimization.

## Chapter 6

## **Future Work**

Experimental work is essential for future work on ammonia synthesis absorption integrated systems, as the amount available in the literature is limited. Experimental work could also shed some light on the assumptions made for simplifications. That could, for example, be the assumption about  $NH_3$ ,  $H_2$  and  $N_2$ , behaving ideally. Or it could be neglect of intermediates.

A thorough economic assessment of the entire system, including one for the Conventional Habor-Bosch process. As this could highlight which parts need improvement for absorption-enhanced ammonia synthesis under mild conditions to be a viable and sustainable alternative to the conventional Haber Bosch process.

Further research on cobalt-promoted Fe-based catalyst and other "cheaper" catalysts that show potential for ammonia-enhanced synthesis. The experimental results of the KATALCO-37 under the "mild" condition showed potential [11].

# Bibliography

- [1] Carlos Arnaiz del Pozo and Schalk Cloete. "Techno-economic assessment of blue and green ammonia as energy carriers in a low-carbon future". In: Energy Conversion and Management 255 (2022), p. 115312. ISSN: 0196-8904. DOI: https://doi.org/10.1016/j.enconman.2022.115312. URL: https://www.sciencedirect.com/science/article/pii/S019689042200108X.
- [2] Mahdi Malmali et al. "Better Absorbents for Ammonia Separation". In: ACS Sustainable Chemistry and Engineering 6 (5 May 2018), pp. 6536–6546. ISSN: 21680485. DOI: 10.1021/acssuschemeng.7b04684.
- [3] Jimmy A. Faria. "Renaissance of ammonia synthesis for sustainable production of energy and fertilizers". In: Current Opinion in Green and Sustainable Chemistry 29 (2021), p. 100466. ISSN: 2452-2236. DOI: https://doi.org/10.1016/j.cogsc. 2021.100466. URL: https://www.sciencedirect.com/science/article/pii/S2452223621000225.
- [4] Collin Smith, Alfred K. Hill, and Laura Torrente-Murciano. "Current and future role of Haber–Bosch ammonia in a carbon-free energy landscape". In: *Energy Environ. Sci.* 13 (2 2020), pp. 331–344. DOI: 10.1039/C9EE02873K. URL: http://dx.doi.org/10.1039/C9EE02873K.
- [5] Us Department of Energy. Potential Roles of Ammonia in a Hydrogen Economy A Study of Issues Related to the Use Ammonia for On-Board Vehicular Hydrogen Storage. 2006.
- [6] Collin Smith and Laura Torrente-Murciano. "Exceeding Single-Pass Equilibrium with Integrated Absorption Separation for Ammonia Synthesis Using Renewable Energy—Redefining the Haber-Bosch Loop". In: *Advanced Energy Materials* 11 (13 Apr. 2021). ISSN: 16146840. DOI: 10.1002/aenm.202003845.
- [7] Deepak K. Ojha et al. "Integrated Ammonia Synthesis and Separation". In: *ACS Sustainable Chemistry and Engineering* 7 (23 Dec. 2019), pp. 18785–18792. ISSN: 21680485. DOI: 10.1021/acssuschemeng.9b03050.
- [8] Line Flansmose Olsen and Elizaveta Taranets. *CFD modelling and optimization of ammonia synthesis-absorption integrated reactor under mild conditions*. eng. 2024.
- [9] Bosong Lin et al. Perspective on Intensification of Haber-Bosch to Enable Ammonia Production under Milder Conditions. July 2023. DOI: 10.1021/acssuschemeng.2c06711.
- [10] Collin Smith, Alon V. McCormick, and E. L. Cussler. "Optimizing the Conditions for Ammonia Production Using Absorption". In: *ACS Sustainable Chemistry and Engineering* 7 (4 Feb. 2019), pp. 4019–4029. ISSN: 21680485. DOI: 10.1021/acssuschemeng. 8b05395.
- [11] Collin Smith and Laura Torrente-Murciano. "Low Temperature and Pressure Single-Vessel Integrated Ammonia Synthesis and Separation using Commercial KATALCO Catalysts: Green ammonia synthesis using renewable energy". In: *Johnson Matthey Technology Review* 66 (4 Oct. 2022), pp. 435–442. ISSN: 20565135. DOI: 10.1595/205651322X16577001040526.

- [12] Collin Smith et al. "Rates of Ammonia Absorption and Release in Calcium Chloride". In: ACS Sustainable Chemistry & Engineering 6.9 (2018), pp. 11827–11835. DOI: 10.1021/acssuschemeng.8b02108. eprint: https://doi.org/10.1021/acssuschemeng.8b02108. URL: https://doi.org/10.1021/acssuschemeng.8b02108.
- [13] Mahdi Malmali et al. "Ammonia Synthesis at Reduced Pressure via Reactive Separation". In: Industrial & Engineering Chemistry Research 55.33 (2016), pp. 8922-8932. DOI: 10.1021/acs.iecr.6b01880. eprint: https://doi.org/10.1021/acs.iecr.6b01880. URL: https://doi.org/10.1021/acs.iecr.6b01880.
- [14] A. Mirvakili et al. "Two-dimensional mathematical modeling of an industrial ammonia synthesis reactor with CFD analysis". In: *Journal of the Taiwan Institute of Chemical Engineers* 121 (Apr. 2021), pp. 1–19. ISSN: 18761070. DOI: 10.1016/j.jtice.2021.03.032.
- [15] Amin Nikzad et al. "Conceptual comparison of three novel configurations in the spherical radial flow reactor for ammonia production". In: *Fuel* 321 (Aug. 2022). ISSN: 00162361. DOI: 10.1016/j.fuel.2022.123945.
- [16] Tianbao Gu et al. "Exploring decentralized ammonia synthesis for hydrogen storage and transport: A comprehensive CFD investigation with experimental validation and parametric study". In: *Energy Conversion and Management* 295 (Nov. 2023). ISSN: 01968904. DOI: 10.1016/j.enconman.2023.117604.
- [17] M.A. Kibria, D.E. McManus, and S. Bhattacharya. "Options for net zero emissions hydrogen from Victorian lignite. Part 2: Ammonia production". In: *International Journal of Hydrogen Energy* 48.95 (2023), pp. 37166–37182. ISSN: 0360-3199. DOI: https://doi.org/10.1016/j.ijhydene.2023.06.098. URL: https://www.sciencedirect.com/science/article/pii/S0360319923029579.
- [18] Md Burhan Kabir Suhan et al. "Optimal design of ammonia synthesis reactor for a process industry". In: *Journal of King Saud University Engineering Sciences* 34 (1 Jan. 2022), pp. 23–30. ISSN: 10183639. DOI: 10.1016/j.jksues.2020.08.004.
- [19] Ali Dashti et al. "Modeling and simulation of ammonia synthesis reactor". In: *Petroleum & Coal* 48.2 (2006), pp. 15–23.
- [20] Louis J. Gillespie and James A. Beattie. "The thermodynamic treatment of chemical equilibria in systems composed of real gases. I. An approximate equation for the mass action function applied to the existing data on the haber equilibrium". In: *Physical Review* 36.4 (1930). Cited by: 56, 743 753. DOI: 10.1103/PhysRev.36.743. URL: https://www.scopus.com/inward/record.uri?eid=2-s2.0-0342883667&doi=10.1103%2fPhysRev.36.743&partnerID=40&md5=a23e8d826f849f8d238903007e067751.
- [21] D. C. Dyson and J. M. Simon. "Kinetic Expression with Diffusion Correction for Ammonia Synthesis on Industrial Catalyst". In: *Industrial & Engineering Chemistry Fundamentals* 7.4 (1968), pp. 605–610. DOI: 10.1021/i160028a013. eprint: https://doi.org/10.1021/i160028a013. URL: https://doi.org/10.1021/i160028a013.
- [22] Chungen Yin. CFD lecture 1 slides. 2023.
- [23] Inc. Ansys. Ansys Fluent Theory Guide, Release 2022 R1. 2021.
- [24] HySTrAm. HySTrAm. url: https://www.hystram.eu/.
- [25] H K Versteeg and W Malalasekera. An Introduction to Computational Fluid Dynamics Second Edition. URL: www.pearsoned.co.uk/versteeg.

- [26] Ismail B. Celik et al. "Procedure for Estimation and Reporting of Uncertainty Due to Discretization in CFD Applications". In: Journal of Fluids Engineering 130.7 (July 2008), p. 078001. ISSN: 0098-2202. DOI: 10.1115/1.2960953. eprint: https://asmedigitalcollection.asme.org/fluidsengineering/article-pdf/130/7/078001/5491455/078001\\_1. pdf. URL: https://doi.org/10.1115/1.2960953.
- [27] D. Frattini et al. "A system approach in energy evaluation of different renewable energies sources integration in ammonia production plants". In: Renewable Energy 99 (2016), pp. 472-482. ISSN: 0960-1481. DOI: https://doi.org/10.1016/j.renene. 2016.07.040. URL: https://www.sciencedirect.com/science/article/pii/S096014811630636X.

## Appendix A

# **Geometry script**

```
1 # Parameters for the reactor
2 reactor_height = Parameters.Diameter_reactor # Height of the 2D reactor (
      originally diameter)
3 inlet_length = 20
                          # Length of the inlet part in mm
5 cat_ab_ratio = 0.5 # Catalyst to absorbent ratio
8 catalyst1_length = 90 * cat_ab_ratio / (cat_ab_ratio + 1) # mm
9 absorption1_length = 90 - catalyst1_length # mm
10 \text{ outlet_length} = 40
12 total_length = inlet_length + catalyst1_length + absorption1_length +
      {\tt outlet\_length}
13
14 # Clear existing geometry
15 part = GetRootPart()
16 if part.Bodies.Count > 0:
17
      for body in part.Bodies:
18
           body.Delete()
19
20 def create_rectangle(x_position, width, height, name):
      new_component = ComponentHelper.CreateAtRoot(name)
22
      ComponentHelper.SetActive(new_component)
23
24
      # Create a sketch on the XY-plane (planar surface for Fluent 2D)
25
      base_plane = Plane.Create(Frame.Create(Point.Create(x_position, 0, 0),
      Direction.DirX, Direction.DirY))
26
      ViewHelper.SetSketchPlane(base_plane)
27
28
      corner1 = Point2D.Create(MM(0), MM(0))
29
      corner2 = Point2D.Create(MM(width), MM(0))
30
      corner3 = Point2D.Create(MM(width), MM(height))
31
      SketchRectangle.Create(corner1, corner2, corner3)
32
33
      ViewHelper.SetViewMode(InteractionMode.Solid, None)
34
35
      # Rename the surface body
36
      body = new_component.Content.Bodies[0]
37
      body.SetName(name)
39 # Create each 2D rectangular section
40 create_rectangle(MM(0), inlet_length, reactor_height, "Inlet")
41 create_rectangle(MM(inlet_length), catalyst1_length, reactor_height, "
      Catalyst Bed1")
42 create_rectangle(MM(inlet_length + catalyst1_length), absorption1_length,
      reactor_height, "Absorption1")
43
44 create_rectangle(MM(inlet_length + catalyst1_length + absorption1_length),
      outlet_length, reactor_height, "Outlet")
```

## Appendix B

# **User Defined Expressions**

```
name definition description input-parameter output-parameter
 2 "Absorbed_frac_NH3" "NH3Absorbed/(NH3produced)" "" #f #t
 3 "FNH3_out" "-MassFlowInt(MoleFraction(species = 'nh3'),['out'])/(17.03061 [
          kg/kmol])" "" #f #f
 4 "H2Conversion" "(MassAve(MassFraction(species = 'h2'),['inlet_body'])*
          MassFlow(['in']) + MassAve(MassFraction(species = 'h2'),['outlet_body'])*
          MassFlow(['out']))/(MassAve(MassFraction(species = 'h2'),['inlet_body'])*
          MassFlow(['in']))" "" #f #t
 5 "Ka" "10**(-2.691122 * log10(T*1[K^-1]) - 5.519265e-5 [K^-1] * T + 1.848863e
          -7 [K^-2] * T**2 + (2001.6 [K] / T) + 2.6899)" "" #f #f
 6 "GHSV" "3127.255 [h^-1]" "" #t #f
 7 "NH3Absorbed" "-Sum(UserMassSource, ['absorption_bed'])" "" #f #f
 8 "NH3produced" "NH3Absorbed-MassAve(MassFraction(species = 'nh3'),['
          outlet_body'])*MassFlow(['out'])" "" #f #f
 9 "P_NH3" "AbsolutePressure*1[kg^-1 m s^2]/100000*MoleFraction(species = 'nh3')
          " "" #f #f
10 "P_atm" "(AbsolutePressure)/101325" "" #f #f
11 "P_eq1_SmithAbso" "1/(exp(42100/(R*1[J^-1 K mol])*(1[K]/(T)-1/650)))**2" ""
12 \ "P_eq2_SmithAbso" \ "1/(exp(42100/(R*1[J^-1 \ K \ mol])*(1 \ [K]/(T)-1/610)))**2" \ ""
             #f #f
13 "Pressure_in" "4000000 [kg m^-1 s^-2]" "" #t #f
14 "Velocity_in" "(GHSV*0.03[m]*0.38[kg*m^(-3)])/(7.148119885[kg*m^(-3)])" "" # \frac{1}{2}
          f #f
15 "R_SmithAbso" "IF(MolarConcentration(species = 'nh3')*17.03061[kg kmol^-1]/dt
          >-1*R_SmithAbso_pre, R_SmithAbso_pre, -1*MolarConcentration(species = '
          nh3')*17.03061[kg kmol^-1]/dt)" "" #f #f
16 "R_SmithAbso_pre" "IF(MoleFraction(species = 'nh3')>0.001,-1[kg m^-3 s^-1]*(
          k_abs_1 + k_abs_2 + k_abs_3*17.03061*600/60,0[kg m^-3 s^-1])" "" #f #
17 "R_abs_heat" "-R_SmithAbso*46e6[J kmol^-1]/17.03061[kg kmol^-1]" "" #f #f
18 "S_H2" "2.01594 [kg kmol^-1]*r_H2" "" #f #f
19 "S_NH3" "17.03061 [kg kmol^-1]*r_NH3_transient" "" #f #f
20 "S_h" "r_NH3_transient*(46.22e6 [J/kmol])" "" #f #f
21 "Xa1" "IF(UDS(uds = 'uds-0') <0.13, UDS(uds = 'uds-0') /0.13, 1)" "" #f #f
22 "Xa2" "IF(UDS(uds = 'uds-1') <0.35, UDS(uds = 'uds-1') /0.35, 1)"
                                                                                                                  "" #f
23 "Xa3" "IF(UDS(uds = 'uds-2')<0.35, UDS(uds = 'uds-2')/0.35, 1)"
24 "YieldNH3" "NH3produced/17.03061 [kg/kmol])/((MassAve(MassFraction(species =
            'h2'),['inlet_body'])*MassFlow(['in']) + MassAve(MassFraction(species =
          'h2'),['outlet_body'])*MassFlow(['out']))/2.01594 [kg/kmol])" "" #f #t
25 "a_N2" "(0.93431737 + 0.3101804e-3[K^-1]*T + 0.29589610e-3 [Pa^-1]*P_atm -
          0.2707279 = -6[K^{-2}]*T**2 + 0.4775207 = -6[Pa^{-2}]*P_atm**2)*P_atm*x_N2/1[Pa]
          " "" #f #f
26 "a_NH3" "(0.1438996 + 0.2028538e-2[K^-1]*T - 0.4487672e-3[Pa^-1]*P_atm -
          0.1142945 \\ e-5[K^-2]*T**2 + 0.2761216 \\ e-6[Pa^-2]*P_atm**2)*P_atm*x_NH3/1[Pa]
          " "" #f #f
27 \ "a_h2" \ "(exp(exp(-3.8402 \ [K^-0.125]*T**0.125 \ + \ 0.541)*1 \ [Pa^-1]*P_atm - (exp(-3.8402 \ [K^-0.125]*T**0.125 \ + \ 0.541)*1]
          (-0.1263 [K^-0.5]*T**0.5-15.980))*1 [Pa^-2]*P_atm**2 + 300*exp(-0.01190 [Pa^-2]*P_atm**2 + 300*exp(-
          K^-1*T-5.941)*(exp(-P_atm/300 [Pa])) ))*P_atm*x_H2/1[Pa]" "" #f #f
```

```
28 "dP" "MassFlowAve(AbsolutePressure,['in']) - MassFlowAve(AbsolutePressure,['
      out'])" "" #f #t
29 "expr1" "MassFlowInt(MassFraction(species = 'nh3'),(['out']))" "" #f #f
30 "expr2" "MassAve(MassFraction(species = 'nh3'),['outlet_body']) * MassFlow(['
      out'])" "" #f #f
31 "expr3" "1+MassFlowInt(MassFraction(species = 'nh3'),['out'])/MassFlowInt(
     MassFraction(species = 'nh3'),['ab_in'])" "" #f #f
32 "k" "8.849*10**14* 1 [kmol m^-3 s^-1] * (1/3600)* exp(-170560 [K^1] / (8.314)
      * T))" "" #f #f
33 \mbox{"k_abs_1" "3e-4*max(0,(P_NH3-0.05))*(1-Xa1)" "" #f #f}
34 "k_abs_2" "2e-2*max(0,(P_NH3-P_eq1_SmithAbso))**4*(1-Xa2)**4" "" #f #f
35 \text{ "k_abs_3" "2.5e-2*max(0,(P_NH3-P_eq2_SmithAbso))**4*(1-Xa3)**6" "" #f #f
36 "r_H2" "-3*r_NH3_transient/2" "" #f #f
37 "r_NH3" "IF(MolarConcentration(species = 'h2') > 0.05 [kmol/m^3], max(0 [kmol = 1.0])
       m^3 s^{-1}, 2*k* ((Ka**2 * a_N2 * (a_h2**3 / a_NH3**2)**0.5) - (a_NH3**2)**0.5)
       / a_h2**3)**(1-0.5))), 0 [kmol m^-3 s^-1])" "" #f #f
38 \text{ "r_NH3\_transient" "IF(MolarConcentration(species = 'h2')/dt/1.5>r_NH3, r_NH3, r_NH3, r_NH3)}
       MolarConcentration(species = 'h2')/dt/1.5)" "" #f #f
39 "r_abso1" "3e-4*max(0,(AbsolutePressure*1[kg^-1 m s^2]/100000*MoleFraction())
      species = 'nh3')-0.05))*(1-IF(UDS(uds = 'uds-0')<0.13,UDS(uds = 'uds-0')
      /0.13,1))/60*125.844*Density*1[s-1]" "#f #f
40 \text{ "r_abso2" "} 2e-2*max(0,(AbsolutePressure*1[kg^-1 m s^2]/100000*MoleFraction())
      species = 'nh3')-P_eq1_SmithAbso))**4*(1-IF(UDS(uds = 'uds-1')<0.35,UDS(
      uds = 'uds-1') /0.35,1)) **4/60*125.844* Density*1[s-1]" "" #f #f
41 "r_abso3" "2.5e-2*max(0,(AbsolutePressure*1[kg^-1 m s^2]/100000*MoleFraction(
      species = 'nh3')-P_eq2_SmithAbso))**4*(1-IF(UDS(uds = 'uds-2')<0.35,UDS(</pre>
      42 "x_H2" "max(MoleFraction(species = 'h2'), 0.005)" "" #f #f
43 \text{ "x_N2" "max(MoleFraction(species = 'n2'), 0.005)" "" #f #f}
```

# Appendix C

# **Optimaztion Canidate Points**

GHSV	Diameter <sub>reactor</sub>	Absorbed Fraction	H <sub>2</sub> conversion
2627.25500000000	10.00000000000000	0.963217617500000	0.0653374246944445
2627.36301784615	44.8178708201185	0.962468779076486	0.0656330758439983
2627.27463636528	19.9633544676844	0.962928795333894	0.0653401515601713
2627.45852369675	45.4625892458848	0.962460349409733	0.0656453250870438
2627.32278835357	37.6706349994206	0.962563122962468	0.0655070744805255
2627.43067104674	22.0831528790100	0.962873218873964	0.0653479213387911
2627.255000000000	10.00000000000000	0.963217617500000	0.0653374246944445
2627.38068901265	25.9548028286638	0.962782749419773	0.0653726341399901
2627.57257132373	41.4186571141374	0.962506380034972	0.0655669918621494
2627.41414972106	25.3820046578417	0.962795229165203	0.0653681312345125
2627.33370282337	30.6678383956586	0.962684726526495	0.0654159927804842
2627.47393855907	38.8426095934099	0.962543428423410	0.0655241908441959
2627.36672257171	36.8603202223382	0.962575065439840	0.0654945119999812
2627.35193329566	21.0597409706961	0.962899764711563	0.0653438276661662
2627.32254250875	28.0805427688077	0.962737352231478	0.0653906834635108
2627.28596443047	36.0001432867169	0.962589999791360	0.0654827333377268
2627.33342052150	24.6518191864986	0.962812985964252	0.0653637532854996
2627.31549073289	23.7089526009863	0.962835291557960	0.0653578897185586
2627.53586701361	44.0914467557817	0.962474239687719	0.0656172240167658
2627.52801830086	39.9361592836004	0.962527039916207	0.0655417199071373
2627.34029198613	21.6123636518684	0.962886012548668	0.0653464117610166
2627.28911500019	23.6121540191809	0.962837916689584	0.0653575293144900
2627.31641379153	38.2700695040669	0.962554170130536	0.0655164256382983
2627.38543197449	33.0067604499568	0.962640050856236	0.0654423330576430
2627.97445915482	26.9734791570019	0.962752615723792	0.0653756343598320
2627.34689324967	43.8317661580599	0.962480128265269	0.0656137700551801
2627.31988844973	30.2515663570907	0.962693082115935	0.0654117236022522
2627.63015140678	29.9395101845119	0.962695133446844	0.0654058772863118
2627.25895541690	41.9777929606141	0.962503912695606	0.0655797052487117
2627.37645462751	35.4513267942427	0.962597742868150	0.0654742689074308
2627.27171782983	22.8001725348137	0.962857620541293	0.0653530200207534
2627.29315686850	31.1765305758273	0.962675432391785	0.0654218529634298
2627.29135829487	40.5509674050940	0.962522109826835	0.0655541890460333
2627.50654208357	42.8803174334165	0.962488964841024	0.0655942661649631
2627.25533291120	19.1041138457969	0.962951550739015	0.0653374764601092

**Table C.1:** Candidate points